Digital Dissemination of Textile Intangible Cultural Heritage Craftsmanship Combined with Digital Twins

Wei ZHAO
Department of Literature, Jiaozuo Normal College, Jiaozuo 454000, Henan, China
Corresponding author: Wei ZHAO (e-mail: ZhaoW9085@126.com)

ABSTRACT Textile intangible cultural heritage preservation faces significant challenges in process reconstruction, semantic continuity, and interactive dissemination. To address these issues, this study proposes a digital dissemination framework that integrates digital twin technology with three-dimensional geometric reconstruction, motion capture, and immersive interaction. High-fidelity models are generated through laser scanning and multi-view photogrammetry, while IMU-based motion acquisition and skeletal animation are employed to restore complex craft operations with dynamic synchronization and predictive correction. The system further combines physics-based simulation, metadatadriven process organization, and a WebXR-enabled interaction platform to establish a closed-loop workflow linking physical behaviors with virtual representations. Considering that modern wearable sensing and digital twin systems increasingly depend on electromagnetic signal acquisition and wireless information transmission, the proposed framework also provides a reference architecture for intelligent sensing platforms involving antenna-assisted communication and multimodal electromagnetic data integration. Experimental results demonstrate a point cloud overlap rate of 94.2%, geometric reconstruction errors as low as 0.47 mm, action synchronization exceeding 90% at key process nodes, and interaction latency below 70 ms under high-load conditions. The proposed approach achieves highfidelity restoration and immersive dissemination of textile craftsmanship while offering valuable technical insights for digital heritage preservation, intelligent wearable systems, and electromagnetic-enabled interactive applications.

INDEX TERMS digital twin, textile intangible cultural heritage, wearable electromagnetic sensing, interactive visualization, motion capture

I. INTRODUCTION

As global cultural heritage protection advances, textile intangible cultural heritage—an essential form of traditional handicrafts—faces challenges in digital dissemination. Its processes rely on tacit knowledge and embodied skills, which static records fail to capture. Insufficient dissemination channels and weakened semantics further constrain accessibility. Current digitization mainly centers on image archiving and text annotations. While useful for preservation, these lack interactivity, coherence, and cultural context [1,2]. Existing methods rely on static visuals and two-dimensional videos, failing to capture dynamic processes and nonverbal knowledge, which hinders public understanding of traditional techniques [3,4]. The expression of weaving motions remains fragmented, disrupting the simulation of operation order, force rhythm, and pattern creation [5,6]. Communication platforms still use basic "image–text + video" formats, lacking immersive and participatory experiences, falling short of digital natives' expectations [7,8].

Data fragmentation, limited modeling depth, and closed interactivity obstruct effective dissemination. These limitations reveal a gap between modeling and dissemination and restrict expressive capacity [9–11]. A digital twin system integrating process modeling, action logic restoration, and communication structure is needed to unify logic, interaction, and semantics [12–14].

Although existing research has advanced digital geometric error, semantic annotation, and immersive presentation, these efforts remain disjointed in their treatment of process logic, cultural semantics, and user interaction. Prior studies predominantly emphasize high-fidelity reconstruction or platform-level visualization. However, they lack a closed operational chain that unifies motion acquisition, semantic encoding, and interactive dissemination. The absence of such integration results in fragmented reproduction of tacit procedural knowledge and insufficient linkage between technical execution and cultural interpretation. The digital twin architecture developed in this study establishes a process-closed framework in which motion trajectories, tool operations, and semantic metadata are dynamically synchronized. By coupling data acquisition, behavioral logic restoration, and interactive dissemination, the proposed approach constructs a coherent communication path that simultaneously preserves technical rigor and conveys cultural meaning, thereby addressing a fundamental gap in current digital preservation methods.

To resolve these issues, this paper builds a digital twin-based communication system for textile intangible cultural heritage. The method integrates dynamic modeling, behavioral data acquisition, and immersive interaction into a process-closed technical structure. Multi-view photogrammetry and laser scanning are first used to collect geometric data of tools and crafts, producing high-fidelity 3D models. IMU-based wearable sensors then capture motion sequences, extract skeletal parameters and keyframes, and construct standardized action timelines. Using the Unity engine, a skeletal animation system is developed and coupled with physics-based simulation to replicate weaving features such as tension and linear swing. For interaction, a browser interface built on WebXR supports real-time model display, path switching, and node-based control using dynamic data streams. A metadata system structures process logic, tool-action mappings, and pattern semantics for semantic querying and data scheduling. Rendering is supported through a MySQL database and Node.js backend, enabling real-time scene configuration and dynamic communication routes.

II. RELATED WORK

Recent studies on digital modeling of textile intangible cultural heritage focus on geometric error, semantic structure, behavior simulation, and visual presentation, forming a multidimensional approach. Wang et al. [15] combined CAD and reinforcement learning to build high-precision models and used VR to enhance immersive display. Liu [16] proposed a comprehensive platform covering collection to dissemination, offering a knowledge-driven logic framework. Ban et al. [17] applied graph neural networks with anisotropic modeling and repulsion loss to improve cloth collision detection and texture restoration. Their Neo-Hookean Saint- Venant–Kirchhoff method enhanced dynamic simulation and mechanical representation [17]. Jing et al. [18] used ontology semantic networks to build digital models of Nanjing brocade, enabling semantic retrieval and supporting knowledge services. Hassan Architecture et al. [19] introduced "hybrid reconstruction," integrating craft features into modeling to improve visual integrity, applicable to textile digitalization. Though progress has been made in geometry, semantics, dynamics, and platform design, an integrated system covering action logic, pattern generation, and knowledge structure with process closure and interactivity remains absent.

Digital twins are key to virtual-real mapping and interactive cultural communication. Researchers explored modeling, semantics, and structural feedback. Chiachío et al. [20] used IoT sensors in structural digital twins to enable real-time feedback, also providing logic for cultural heritage twins. Luther et al. [21] reviewed virtual museums and developed a metadata-driven twin construction method, supporting content integrity and collaboration in dissemination. Amelio et al. [22] proposed a semantic-model-based "digital cultural heritage twin," using narrative knowledge language to enhance cultural expression, aiding symbolic textile heritage modeling. Shabani et al. [23] combined photogrammetry and laser scanning with finite element analysis for structure evaluation, offering a path for modeling textile artifacts. Ning [24] integrated digital twins with 3D modeling to construct complete ICH scenes, using multimedia and feature extraction to enhance expression. Despite rich exploration, a closed-loop system unifying dynamic logic, semantic chains, and feedback in textile heritage is still lacking.

III. DESIGN OF PROCESS REPRODUCIBILITY SYSTEM DRIVEN BY DIGITAL TWIN

3D MODELING MODULE DESIGN

The digital twin modeling of textile intangible cultural heritage relies on high-fidelity geometric reconstruction. In the 3D modeling module, geometric data of weaving tools and fabrics were acquired using laser scanning and multi-view photogrammetry. Laser scanning provided dense point clouds, and by adjusting scanning paths and intervals, captured fine structural details with millimeter-level precision. In this process, the scanning interval was set to 0.3 mm with a rotation step of 0.5° to achieve uniform coverage of fabric and tool surfaces. In the ICP registration stage, the neighborhood radius was normalized according to the mean point spacing, and the effective search range was constrained to within several multiples of the average nearest neighbor distance in order to avoid mismatch caused by scale inconsistency. A k-nearest-neighbor (k-NN) strategy combined with a robust kernel weighting function was employed to suppress the influence of non-uniform sampling density. The search radius was set to 0.1 m as the upper bound of correspondence search, the number of iterations was limited to 50, and convergence was determined by a residual reduction ratio with a termination threshold of 10^{-3}. The nearest-neighbor ratio was treated as a dimensionless parameter representing the proportion of valid correspondences, while the outlier removal threshold was expressed in millimeters to bound the maximum admissible residual. These parameter definitions established a scale-consistent and noise-resistant registration environment that ensured the stability of multi-source point cloud fusion. Photogrammetry, assisted by structured light, synchronously collected images and applied Structure-from-Motion (SfM) and Multi-View Stereo (MVS) algorithms to generate textured mesh models. A weighted-error–based point-cloud registration aligned laser and image data, improving geometric accuracy and mesh topology closure. The registration error function is defined as:

$$E_{\text{err}} = \sum_{i=1}^{N} w_i \left\| P_i^{\text{laser}} - R \cdot P_i^{\text{photo}} - t \right\|^2 \tag{1}$$

P_i^{laser} and P_i^{photo} represent the corresponding points obtained by laser scanning and photogrammetry, respectively. w_i is the confidence weight. R and t are the rotation matrix and translation vector, respectively. ICP (Iterative Closest Point) is used to optimize the solution, minimizing the overall registration error iteratively.

After registration, the multi-source point-cloud data underwent normal estimation and Poisson surface reconstruction to generate a topologically consistent closed mesh. Boundary reshaping ensured overall physical continuity. During texture mapping, multi-view images were projected onto the mesh, and weighted fusion was applied based on illumination and view coverage to create a high-resolution texture map, achieving geometry–texture integration.

Figure 1 shows the modeling path and data flow hierarchy, illustrating the transitions from raw sampling to 3D model generation, including image processing and point cloud fusion. It outlines the full-process framework for high-precision digital twin construction. This framework serves as the foundation for subsequent modules of motion acquisition, behavior simulation, and interactive communication.

The generated 3D model had to be parameterized after modeling to accommodate the subsequent bone binding and physical simulation processes. The mesh simplification algorithm was used to construct the LOD (Level of Detail) layered structure of the high-density model, compressing the redundant faces while maintaining the geometric fidelity of the detail area and generating multi-level model versions for layered loading and real-time rendering. The model topology optimization applied edge folding and edge exchange strategies and controlled the geometric offset through the error tolerance function:

$$\Delta_{\text{geo}} = \max_{v \in \partial M} \| v - \Pi_S(v) \| \tag{2}$$

Δ_{geo} is the upper bound of the simplification error; ∂M is the set of original boundary vertices; and Π_S represents the nearest point projection operator from the simplified model surface to the original model boundary.

During semantic segmentation, the tool structure is divided using geometric feature clustering to extract key components such as the shuttle and spinning wheel. Mesh labeling enables metadata annotation and structured retrieval. The model was then converted to FBX format and imported into Unity with topology, material, and partition labels to ensure coordinate consistency and support bone binding.

MOTION ACQUISITION AND DRIVE SYSTEM

To capture the dynamic operation of textile intangible cultural heritage and drive 3D animation, the system integrates IMU sensing with skeletal animation. This module includes wearable sensors, a posture-solving algorithm, data standardization, and skeleton binding, forming a closed loop from motion capture to virtual mapping.

IMUs with accelerometers, gyroscopes, and magnetometers were placed at joints to collect tri-axial acceleration, angular velocity, and magnetic signals. A total of fifteen nodes were arranged to cover the wrists, ankles, upper arms, thighs, sternum, and lower back, forming a complete skeletal acquisition array. Each device was calibrated through a static T-pose before recording. The sensor weight w_i in Equation (3) was initialized from the nominal accuracy values provided by the hardware specifications and subsequently updated according to the variance of real-time signals within a sliding window, so that lower-noise channels contributed higher weights in the fusion process. After quaternion-based posture solving, Euler-angle bone rotation vectors were serialized by timestamp. Kalman filtering and zero-speed updates were used to reduce noise and drift, enabling accurate motion reconstruction:

$$R_t = \text{Exp}\left(\sum_{i=1}^{M} w_i \cdot \log\left(R_i^t\right) \right) \tag{3}$$

R_t is the rotation matrix of the target bone at time t; R_i^t is the rotation matrix output by the i-th IMU; and w_i is the sensor weight.

The filtered data were mapped to the virtual skeleton and were simultaneously fed back to recalibrate sensor parameters in real time, forming a closed-loop mechanism in which physical deviations continuously refine virtual behavior and predicted trajectories, thereby achieving sustained bidirectional synchronization. The collected data were mapped to the 3D model's skeleton using the Humanoid template. Unity's Animator module drives real-time posture changes via skeleton rotation vectors, restoring weaving actions dynamically. To ensure timing and amplitude accuracy, a trajectory compensation mechanism calibrates differences between IMU data and virtual motion paths. The error function is expressed as:

$$E_{\text{traj}} = \frac{1}{T} \int_0^T \| x_{\text{real}}(t) - x_{\text{virtual}}(t) \|^2 \, dt \tag{4}$$

x_{real} is the joint trajectory in the sensor space; x_{virtual} is the model virtual space trajectory; T is the total action time, and the degree of simulation is improved by minimizing the difference through the trajectory fitting function. Trajectory fitting was implemented through a piecewise cubic Hermite interpolation to preserve continuity of both displacement and velocity across synchronized timestamps. The optimization objective minimized squared deviations between the sensor-space and model-space trajectories, with an additional regularization term constraining angular acceleration to sup-

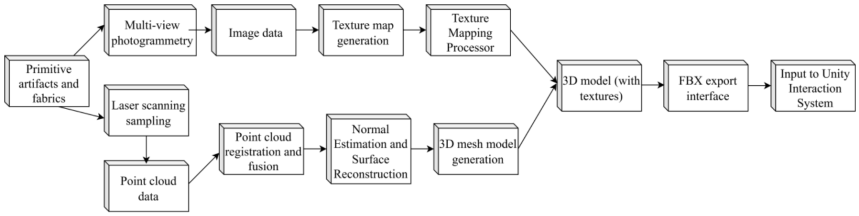

FIGURE 1. System data flow diagram

press oscillatory artifacts. Iterative least-squares solution was applied with a tolerance of 10^{-4} to ensure smooth convergence.

The system supported multi-node synchronization via time-synchronization protocols and global timestamps to ensure correct frame alignment. A buffer queue between acquisition and rendering modules maintained inter-frame stability and real-time response. The graphics module used a state machine to map keyframes to animation states, forming a dynamic input–visual–output chain.

To achieve linkage mapping with subsequent process semantic data, each skeletal path in the system is assigned a unique identification code and a joint motion type label, enabling the construction of a binding semantic relationship matrix. The skeletal action metadata is associated with the process step nodes through a mapping function to establish a three-dimensional index structure of "action–operation–tool", and its conversion function form is as follows:

$$M(i,j,k) = \begin{cases} 1, & \text{if bone } i \text{ participates in operation } j \\ & \text{using tool } k, \\ 0, & \text{otherwise.} \end{cases} \tag{5}$$

$M(i,j,k)$ indicates whether skeleton i has a direct interaction relationship with tool k in process operation j. This structure serves as the basic logical index for matching actions and procedures in process simulation.

PROCESS BEHAVIOR SIMULATION MODELING

To reconstruct and simulate textile intangible cultural heritage operations, the system builds a behavior scene in Unity, integrating skeleton drive, physics, and interaction mechanisms. It maps multi-source data to realistic process contexts, ensuring temporal, structural, and semantic consistency.

Input includes bone-driven motion data and high-precision 3D models. Skeleton joints are animated by frame angle sequences, while models provide collision boundaries. The simulation combines rigid body and cloth dynamics—covering linear, rotational, and flexible behaviors—to ensure realistic tool–fabric interaction. All actions follow a unified coordinate system and absolute time steps. The core control functions are as follows:

$$F_i(t) = m_i \cdot a_i(t) + \sum_{j=1}^{N} R_{ij}(t) + G_i \tag{6}$$

$F_i(t)$ represents the total force acting on node i; m_i is the node mass; $a_i(t)$ is the instantaneous acceleration; $R_{ij}(t)$ is the constraint reaction force with the adjacent node j; and G_i is the gravity term. The skeletal animation system applies a multi-layer state machine architecture, divides the action state according to the process step stage, and constructs the behavior conversion path through the parameterdriven mechanism. To enhance predictive capability, the system incorporates trajectory fitting and error propagation analysis to anticipate forthcoming deviations and pre-adjust animation parameters, thereby reducing latency between physical operations and virtual rendering. The state switching is based on the frame count, trigger conditions, and spatial position dynamic scheduling, and the internal behavior decision logic of the system is expressed as:

$$S_{t+1} = \delta(S_t, \theta_t, p_t) \tag{7}$$

S_t represents the current skeleton animation state; θ_t is the skeleton angle input; p_t is the interactive position parameter; and δ is the state transfer function. The state transfer is constrained by the integrity and logical consistency of the action sequence to prevent frame skipping in non-continuous process behaviors and ensure the complete closure of process visualization.

To link operational actions with object responses, all tools and fabrics are bound to collision bodies that react to posture changes and deformation. A hybrid of Mesh Collider (defining contours) and Spring Joint (providing deformation feedback) forms a constrained interactive feedback mechanism. In the simulation engine, the deformation of the cloth is expressed as the following tension model:

$$E_{\text{cloth}} = \sum_{(i,j)\in\mathcal{E}} k_s \cdot \left(\|x_i - x_j\| - l_{ij}\right)^2 + k_b \cdot \theta_{ij}^2 \tag{8}$$

x_i and x_j are node positions; l_{ij} is the initial length; θ_{ij} is the folding angle; k_s is the tension coefficient; and k_b is the bending coefficient. The overall tension energy function is used to maintain the stability of the fabric shape and avoid non-physical deformation.

STRUCTURING OF METADATA OF CRAFT PATTERNS AND TECHNIQUES

Craft patterns and technical data embody the structural logic and cultural encoding of weaving heritage. Based on synchronized 3D models and action sequences, the system builds a metadata framework through layered coding and semantic modeling to enable semantic expression, behavior control, and cross-platform interaction. The metadata adopts a three-dimensional fusion: operation process as the axis, pattern logic as structure, and tools as nodes, forming a searchable weaving knowledge map.

At the data layer, a tree-like operation graph decomposes techniques into units, representing execution order, dependencies, and concurrency via node attributes and directed edges to construct a complete process chain. The definition of operation nodes was derived from synchronized IMU keyframes and multi-view recordings, which were cross-validated by domain experts. Dependencies were identified through temporal overlap analysis, with concurrent actions marked when their keyframes occurred within a 200 ms interval, and strictly sequential steps recorded as directed edges. The attribute set of each node was completed by combining human annotation with algorithm-based feature extraction, ensuring semantic integrity while retaining computational efficiency. The graph structure node attributes are defined as five-tuples as follows:

$$N_i = \langle A_i, T_i, O_i, M_i, R_i \rangle \tag{9}$$

A_i represents the action type to which the node belongs; T_i is the action duration; O_i is the associated tool object index; M_i is the pattern change identifier; and R_i is the local weaving result mapping function generated by this step.

For pattern structure analysis, the system builds a pattern encoding table using texture maps and unit pattern extraction. Hash index compression encodes generation parameters and spatial rules. The table supports modular reuse, symmetry transformation, cross-technique reconstruction, and simulates pattern repetition and gradients via image matrix transformations. Its core expression is as follows:

$$P(x, y) = \sum_{k=1}^{K} \alpha_k \cdot f_k(x, y) \tag{10}$$

$P(x, y)$ represents the pixel value of the pattern on the two-dimensional plane; $f_k(x, y)$ is the k-th pattern function primitive; and α_k is its activation weight at that position. By controlling the rules of α_k changing with coordinates, the parametric generation of multi-technique mixed patterns is realized, and it is bound to the cloth grid in Unity for real-time update.

In terms of the linkage between metadata and animation behavior, the system utilizes a state machine structure as an intermediary to map the action code in the metadata to the skeletal animation state set. It then employs an interpolation function to establish the inter-frame action transition path, ensuring the visual coherence of each technique process. The state synchronization function uses time, tool position, and behavior target as trigger conditions to construct a joint conditional expression:

$$S_t = \gamma(\psi(t), \eta(t), \chi(t)) \tag{11}$$

$\psi(t)$ is the metadata index corresponding to the current time step; $\eta(t)$ is the tool interaction state identifier; $\chi(t)$ is the user control variable set; function γ outputs the system state transfer logic and triggers the corresponding animation or pattern generation operation.

COMMUNICATION PLATFORM DESIGN BASED ON EMBODIED INTERACTION

The immersive platform, built on WebXR, enables dynamic rendering and real-time interaction of weaving processes in the browser. Its architecture includes a scene renderer, behavior module, and data adapter to manage models, metadata, and user input for cross-device 3D display. Event-driven logic with frame-level listeners forms a closed-loop response chain.

Rendering relies on Unity's WebGL export. After resource compression, it loads models, binds skeletal actions, and maps metadata in real time. WebSocket ensures two-way synchronization with the backend, supporting live data updates during interaction.

In the interaction mode design, the platform supports spatial operation mapping based on six degrees of freedom (6-DoF) input devices. User behavior is mapped to standard input events through event listeners and transmitted to the system. The spatial position, gesture action, and timestamp are standardized and reencoded through the state middle layer to form a ternary interaction control tuple:

$$U_t = \langle P_t, G_t, \theta_t \rangle \tag{12}$$

P_t represents the spatial position vector; G_t is the recognition gesture code; θ_t is the action state identifier corresponding to the current interaction moment. The system matches the process metadata node based on this tuple and triggers the animation, pattern change, or semantic annotation update. Interaction delay optimization is achieved through asynchronous loading, graphics-level caching, and GPU buffer preprocessing; furthermore, a bidirectional prediction function is also inserted between event activation and feedback, thereby enhancing inter-frame smoothness.

The platform's internal behavior triggers build a process flow expression model based on the state diagram mechanism. The mapping relationship between user interaction intentions and process nodes is parsed through a finite state automaton, and the state transfer function is defined as follows: $\delta : Q \times \Sigma \rightarrow Q$, where Q is the set of process states, Σ is the set of user interaction events, and function δ represents the new state to which the current state transfers after receiving an event. The platform dynamically schedules skeletal animation and material binding based on this to achieve staged expression of the process flow.

To support access and interaction from different terminals, the platform builds a unified resource scheduling interface layer, sets hierarchical interaction strategies and perspective switching logic for HMD (Head- Mounted Display) devices, desktop browsers, and mobile terminals, and controls the view zoom ratio and pattern detail loading level through responsive layout and resolution-adaptive functions. The parameter control function determines the specific allocation strategy:

$$R(x, y, d) = \phi(x, y) \cdot \rho(d) \tag{13}$$

$R(x, y, d)$ is the view rendering ratio function; $\phi(x, y)$ represents the resolution normalization factor; $\rho(d)$ is the device type mapping function, which controls the loading strategy between different devices in the interaction level and pattern accuracy.

The platform architecture diagram illustrates the relationships between the input signal flow, process metadata parsing flow, animation rendering flow, and network communication flow. Figure 2 is the operational structure diagram of the immersive interaction platform, illustrating the synchronization mechanism and call chain of the data flow within each module of the client.

In the behavior control layer, the platform builds a multilevel index linking user actions to semantic nodes. User commands trigger process semantics and update pattern and tool status. Each interaction executes a state update to maintain consistency with the process flow. Parsed behaviors are fed to the logic layer and recorded in the database, forming a behavior-indexed process call system.

BACKEND DATA RETRIEVAL AND SERVICE INTERFACE

The backend system, built on MySQL and Node.js, supports structured storage, unified retrieval, and highfrequency services for intangible heritage data. It defines five core tables—components, actions, patterns, semantics, and user behavior—linked via primary and foreign keys. Node.js with Express provides RESTful APIs, using a MySQL connection pool for concurrent request handling. Requests are divided into static (e.g., process definitions) and dynamic (e.g., real-time actions). Static queries use B+ tree indexes; dynamic ones use hash tables and double buffer stacks for rapid response. Middleware employs asynchronous I/O with cache prefetching to boost performance and reduce load.

During API calls, user tokens and status codes in headers determine access rights and operation stage. POST/GET requests are routed, validated, and returned as JSON (JavaScript Object Notation) to the front end via unified routing. The unified data transmission structure defined in the system is:

$$D_{i,j}(t) = \psi(E_i, A_j, \tau_t) \tag{14}$$

$D_{i,j}(t)$ represents the data transmission structure generated by entity E_i corresponding to action A_j at time point t, and function ψ represents the data splicing function, which is used to aggregate semantic tags, skeletal postures, and process state quantities.

In the action data service call, the backend designs the action chain queue cache strategy. It records the action meta-parameters of each stage in the sliding window in a blockchain structure, forming a continuous chain in the dynamic process. The action state transfer model in the sliding window is:

$$S_{t+1} = f(S_t, \Delta A_t) \tag{15}$$

S_t is the process state of the system at time t; ΔA_t is the action differential vector during this period; and function f defines the state transfer rule to maintain the consistency of process logic and the restorability of operation flow.

To support multi-platform access, the backend deploys a multi-protocol gateway enabling dual-channel communication via HTTP (Hypertext Transfer Protocol) and WebSocket. WebSocket handles real-time, twoway data push for high-frequency actions, while HTTP manages structured and historical data queries. An asynchronous coroutine pool allocates threads based on priority, ensuring timely response for key interactions.

To address the scalability requirements of large-scale intangible cultural heritage data and high concurrency conditions, the backend architecture incorporates horizontal extension mechanisms. The database layer adopts partitioning strategies and read–write separation to distribute query load while preserving transactional consistency. Redis is integrated as a distributed cache to accelerate frequent queries and reduce lock contention within the database. Node.js services operate in cluster mode combined with asynchronous coroutine pools, ensuring parallel execution across processor cores and improving system throughput. Message queues are positioned between the application layer and the persistence layer, buffering intensive write operations and mitigating the impact of peak traffic surges. These architectural measures establish an elastic service framework that sustains stable response performance during high-frequency access and continuous data streams generated by multi-source acquisition devices.

IV. SYSTEM CONSTRUCTION AND EXPERIMENTAL PREPARATION

HARDWARE PLATFORM AND DEVELOPMENT ENVIRONMENT

The system construction integrates multiple types of heterogeneous devices and software environments, covering geometry acquisition, motion capture, modeling simulation, interactive rendering and service deployment. 3D modeling used high-precision laser scanning (0.1 mm) and multiview photography, with a 360° turntable and a unified light source. The image was reconstructed in the NVIDIA RTX 4090 environment through Meshroom and RealityCapture, and then mesh optimization and UV unfolding were completed by Blender. Motion data acquisition relied on the IMU device based on inertial navigation to build a 15-node skeleton array with a sampling frequency of 120 Hz. It was transmitted to the local cache via Bluetooth 5.0, and posture solution and skeleton mapping were performed through Python scripts. Processing was performed on an

AEM JOURNAL.ORG

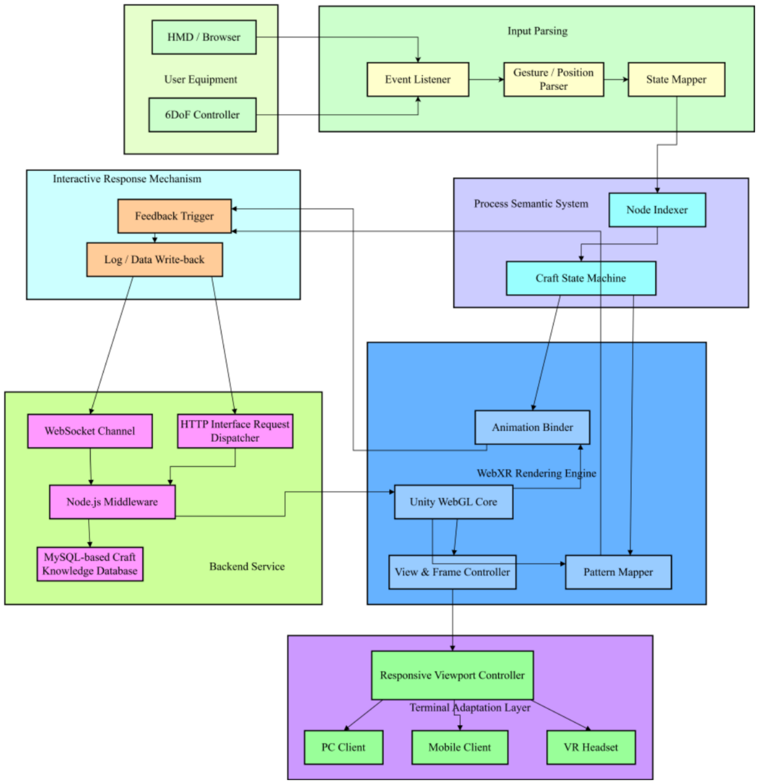

FIGURE 2. Immersive interactive platform operation structure diagram

Intel Core i9-13900K with 64 GB DDR5 memory. Unity 2022.3 LTS (Long-Term Support) was used for simulation and interaction development. FBX models were loaded and NVIDIA PhysX was integrated to achieve physical feedback. HDRP (High Definition Render Pipeline) was used for rendering pipelines. C# logic was developed through Visual Studio 2022. OpenXR Toolkit and WebXR Exporter were integrated. Tests were completed on Chrome, Firefox, and Meta Quest 3. Data were synchronized via USB Type-C, and the frame rate and latency were recorded. The backend was deployed on Ubuntu 22.04, with Node.js 20 and the Express framework. The backend ran on an AMD EPYC 7742 with 128 GB of memory to support highconcurrency processing. The database was MySQL 8.0, which worked with Redis to improve cache response. In order to further support scalability under experimental and potential large-scale deployment scenarios, container-based orchestration was employed for the management of backend services. This approach enabled modular scaling of data storage, cache, and service interfaces. Load balancing mechanisms distributed requests evenly across service instances, while continuous monitoring of latency, throughput, and resource utilization provided feedback for adaptive resource allocation. These strategies collectively formed a foundation that ensured service consistency and operational stability as the scope and diversity of intangible cultural heritage data increase. GPU (Graphics Processing Unit) nodes centrally processed graphics and motion solutions. The frontend and backend used HTTPS and AES-256 for encrypted communication. The system's built-in event listener automatically recorded user behavior to the MySQL database, including timestamps, interaction types, and terminal information, and was linked with the questionnaire system to form a complete experience evaluation chain.

Overview of Intangible Cultural Heritage Craft Samples and Collection Process The selected samples of intangible cultural heritage crafts were representative, complex in structure, and tool-dependent, covering four major national-level projects, including weaving, jacquard, embroidery, printing and dyeing, and spinning. The collection process was screened according to the degree of process closure, action diversity, and semantic relevance to ensure the systematic nature of the data at the action, artifact, and semantic levels. An operation annotation file was established for each type of craft, covering the entire weaving cycle, and two types of node annotation mechanisms were set: rhythm control (such as starting, turning, and deceleration) and structural process (such as warp threading, weft beating, shuttle change, etc.). IMU data and multi-view videos were collected simultaneously at a frequency of 120 Hz, combined with standard action templates and numbering systems to ensure logical consistency and data adjustability. Each craft type was recorded in three sessions under identical conditions, with recalibration carried out prior to every recording. This repeated acquisition maintained consistency across datasets and supported cross-validation of temporal alignment between IMU streams and multi-view video sequences. The collected data were partitioned into training and validation subsets in a 70:30 ratio to establish a reproducible experimental basis. Artifacts were modeled using laser scanning and photogrammetry to provide a basis for subsequent semantic expression. The entire collection cycle lasted 4 weeks and was completed at the intangible cultural heritage inheritance practice base. The sampled data were classified and uploaded to the local server, and a hierarchical path structure was constructed for easy retrieval and invocation. To present the distribution characteristics and data basis of the sample composition in this study, Table 1 lists the main attribute statistics of the process type, including project name, number of actions, number of tools, and total number of frames collected, thereby clarifying the data distribution and system generalization basis.

TABLE 1. Statistical table of attributes of intangible cultural heritage craft samples

Project Name	Number of Actions	Number of Tools	Total Frames Collected
Yun Brocade Weaving	38	12	192,000
Miao Embroidery Blend	31	9	158,400
Zhuang Brocade Jacquard	35	10	176,800
Homespun Cloth Weaving	27	7	144,000
Dong Double-Strap Weaving	25	6	137,600
Plain Embroidery	29	8	148,800
Kesi Silk Weaving	34	11	168,000
Blue Calico Printing	28	7	152,400
Hand Dyeing	30	8	160,800
Spinning	26	6	140,800

SYSTEM MODULE TECHNICAL PARAMETER CONFIGURATION

The system modules are divided into three subsystems according to tasks: data acquisition, modeling and simulation, and interactive presentation. The unified configuration ensures the stability, accuracy, and reproducibility of the platform in a multi-terminal environment. The data acquisition end is equipped with 0.1 mm precision laser scanning and 120 Hz IMU capture device, which cooperates with multi-view images for posture calibration, and combines the industrial-grade calibration system and self-developed preprocessing tools to complete format conversion and denoising. Modeling and simulation are based on Unity 2022.3 LTS, supporting HDRP rendering, HumanIK-driven bone structure, and NVIDIA PhysX 4.1 physical response. Pattern generation uses custom Shader and texture control logic to adapt to various weaving methods. The interactive system is based on the WebXR framework, using a Chromium-based browser that supports WebGL 2.0 and a Three.js event model, and synchronizes data through WebSocket. The backend uses Node.js 20 to build a transmission interface, and MySQL 8.0 to complete the structured storage and scheduling of the process knowledge base.

V. EXPERIMENTAL RESULTS ANALYSIS

ANALYSIS OF 3D MODEL RECONSTRUCTION ACCURACY

To evaluate 3D modeling strategies for textile intangible cultural heritage, this study designed a five-dimensional comparison: (1) sampling density (0.3 mm, 0.5 mm, 1.0 mm); (2) view count (4, 8, 12 views); (3) reconstruction algorithm (OpenMVS, COLMAP, NeRF (Neural Radiance Field)); (4) mesh optimization (none, smoothing, denoising); and (5) occlusion handling (none, texture completion, depth interpolation). Performance was assessed using point cloud overlap, geometric error, ΔE color difference, and synchronization rate, all defined through explicit quantitative formulas. Point cloud overlap was calculated as a three-dimensional voxel-based intersection-over-union, where the common occupied voxel set was divided by the union of the occupied voxel sets of the two models, ensuring consistency across different density distributions. Geometric error was computed as the mean Euclidean distance between paired points after registration, with outliers above two standard deviations excluded through an occlusion mask to maintain statistical stability. Color difference was quantified using the CIEDE2000 ΔE formula, with light and white balance corrected through reference color charts captured under the same illumination conditions, and the calculated ΔE values were reported as average deviations across corresponding texture regions. Synchronization rate was measured as the proportion of correctly aligned motion frames over the total number of annotated frames, with alignment determined by a temporal tolerance of ten milliseconds and validated by dual-stream timestamp comparison. Each metric was reported together with the sampling density, the masking rules applied to occluded areas, and the statistical thresholds used for outlier rejection, ensuring reproducibility of the evaluation process. Table 2 details parameter settings; results are shown in Figure 3. Setup 1, Setup 2, and Setup 3 in each dimension simply represent three independent sets of settings within that dimension and do not form a unified quality level across different dimensions.

TABLE 2. Correspondence table of each setting item in the 3D geometric error assessment diagram

Modeling Dimensions	Setup 1	Setup 2	Setup 3
Dimension 1	0.3 mm	0.5 mm	1.0 mm
Dimension 2	4 Views	8 Views	12 Views
Dimension 3	OpenMVS	COLMAP	NeRF
Dimension 4	No Optimization	Basic Smoothing	Mesh Refinement and Denoising
Dimension 5	No Handling	Texture Completion	Depth Interpolation

Different modeling strategies yield varied 3D expression results. High-density sampling achieves a 94.2% point cloud overlap rate, significantly outperforming 0.5 mm and 1.0

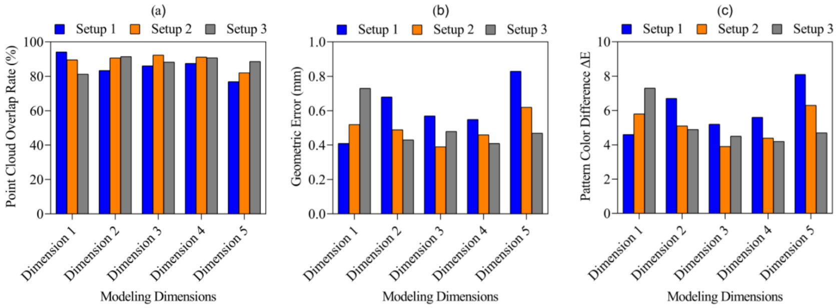

FIGURE 3. Comparison of the impact of different strategies on the three-dimensional expression accuracy in the textile intangible cultural heritage modeling stage. (a) Point cloud overlap rate comparison, (b) Geometric error comparison, (c) Pattern color difference ΔE comparison

mm resolutions due to better surface detail capture. In view configuration, although more perspectives generally improve results, the 12-view setup increases overlap by 0.8% over 8 views. Redundant edge perspectives introduce registration error, offsetting the expected gain from additional viewpoints. Among reconstruction algorithms, COLMAP performs best at 91.2% overlap, surpassing OpenMVS and NeRF. This advantage is attributable to its stable multi-view bundle adjustment, which reduces reprojection error accumulation and ensures more consistent geometric alignment. Occlusion handling also affects geometric accuracy—depth interpolation reduces error to 0.47 mm, over 0.3 mm lower than no processing, showing its role in maintaining shape continuity. For pattern fidelity, sampling density impacts ΔE significantly—coarse sampling reaches 7.3, while fine sampling lowers it to 4.6. NeRF, despite its theoretical advantage, has higher ΔE than COLMAP, indicating that neural methods still suffer from color resampling errors in fine texture reconstruction. These results reveal layered differentiation across strategies, driven by mechanisms such as structural density, viewpoint redundancy, and pattern reconstruction behavior.

PROCESS ACTION SIMULATION RESTORATION

To assess the digital twin system's dynamic restoration performance, eight representative textile crafts were selected: brocade (T1), embroidery (T2), spinning (T3), printing and dyeing (T4), kesi (T5), homespun (T6), blue printed cloth (T7), and Miao embroidery (T8). Each craft varied in structural complexity—e.g., brocade was tightly arranged, embroidery involved fine hand movements, spinning is rhythmic and continuous, and Kesi featured precise multi-track transitions. Miao embroidery shows irregular motions, while homespun and blue cloth are simpler. As shown in Figure 4, five key action nodes were defined: start (D1), acceleration (D2), turning (D3), deceleration (D4), and end (D5), corresponding to motion clarity, rhythm stability, and response flexibility. Trajectory deviation (Fig. 4a) evaluates spatial accuracy; frame synchronization (Fig. 4b) measures rhythmic alignment. These indicators jointly reflect the system's ability to reproduce motion flow across different weaving processes.

Embroidery and Miao embroidery show low median trajectory deviations (3.61 mm and 4.88 mm) due to their short, controlled motion paths. In contrast, spinning and blue printed cloth exceed 7 mm, attributed to multiple force points and large motion amplitudes during continuous operations. Brocade and kesi, though mechanically driven, exhibit moderate deviations due to complex multi-axis coordination, highlighting challenges in simulating coupled structures. The radar chart shows that brocade achieves over 90% frame synchronization at acceleration, turning, and deceleration, indicating strong coherence and system responsiveness. Miao embroidery falls below 76% at start and end, reflecting the difficulty of modeling irregular, nonlinear actions. In general, structured, repetitive crafts yield better restoration and synchronization, while high-freedom techniques increase simulation error. The results indicate not only visual consistency but also the effectiveness of continuous twin synchronization, in which the predictive adjustment mechanism preserves high coherence between physical actions and virtual representations under irregular operational conditions.

USER INTERACTION RESPONSE PERFORMANCE

Under varying resource loads, user interaction performance is influenced by both task type and resource structure. This section evaluates system responsiveness and stability across five high-frequency interaction tasks: model rotation (T1), canvas dragging (T2), pattern loading (T3), perspective switching (T4), and animation playback (T5). Figure 5(a) compares their response delays under low, medium, and high loads, indicating the system's adaptability. Figure 5(b) presents frame rate stability using five metrics: average frame rate, minimum frame rate, coefficient of variation (CV), stability rate, and fluctuation proportion. Figure 5(c) focuses on the resource triggering process, showing the time-consuming structure of five types of loading events, including home page model loading (L1), entering the weaving interface (L2), importing the pattern package (L3), activating the physical simulation module (L4), and initializing the control panel (L5), in the subprocesses of database response (R1), pattern binding (R2), physical initialization (R3), and listener establishment (R4), reflecting the pressure

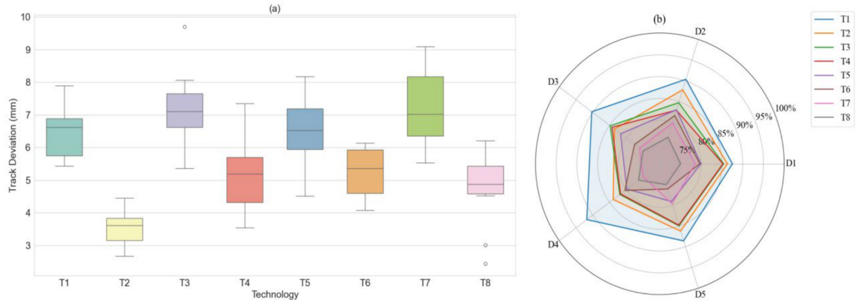

FIGURE 4. Analysis of the digital twin restoration performance of textile intangible cultural heritage technology. (a) Trajectory deviation comparison, (b) Frame synchronization rate radar chart

distribution of different resource types on loading performance. The missing column in Figure 5(c) indicates that the number of executions of the corresponding subprocess of the loading event in the monitoring log is zero. The subprocess is not called under this event path, so no time-consuming record is generated.

In the response delay test, loading pattern operations under high-resource load reached 142 ms— significantly higher than other tasks—likely due to complex data structures and heavy resource binding. In contrast, model rotation maintained sub-70 ms delays across all load levels, indicating low computational demand despite real-time requirements. Frame rate analysis shows loading patterns averaged 52.8 fps, with a 13.4% coefficient of variation (CV) and 16.7% fluctuation rate, reflecting high rendering pressure and poor stability. Model rotation held 59.2 fps with CV under 8%; this indicates strong stability. Entering the weaving interface took 258 ms, with pattern binding and database response comprising nearly two-thirds of that time, making UI coordination and polymorphic pattern scheduling key bottlenecks. Activating the physical simulation module took slightly less time, but over 60% was spent initializing physical parameters—also a major load factor. Overall, interaction performance bottlenecks stem from operational complexity and tight resource coupling. Optimization should focus on simplifying resource structures and separating high-load subprocesses.

PLATFORM OPERATION STABILITY

To assess system stability under multi-platform deployment, five platforms were tested: desktop (P1), WebXR (P2), mobile (P3), embedded (P4), and LAN (P5), each with distinct performance profiles. Desktops offered strong processing power for high-frequency tasks; WebXR ensured accessibility but had limited resource control; mobiles were easy to deploy but compute-limited; embedded devices faced performance and faulttolerance constraints; LAN setups provided stable transmission and sustained performance under load. Five load levels (Light load L1, medium-light load L2, medium load L3, medium-high load L4, heavy load L5) simulates usage from light browsing to high-concurrency operations. Metrics include average operating time (h), crash rate (%), and packet loss rate (%). Figure 6 presents the distribution of these indicators across all platform-load combinations.

System runtime depends on both platform performance and load level. Under heavy load, desktops maintain over 5 hours, while WebXR drops to 3.8 hours due to limited browser resource scheduling. Embedded platforms show rapid runtime decline across all loads, reflecting low stress tolerance from limited hardware and inefficient thread management. Crash rates also vary: desktops and LAN remain below 6% even under stress, while WebXR and embedded platforms exceed 10% after medium load, indicating high environment dependency and the need to optimize Web resource release. Packet loss rates follow similar trends—LAN maintains under 3% even at high load, due to low latency and stable links. Overall, LAN and desktop platforms demonstrate superior runtime and reliability under load, making them optimal choices for sustained deployment.

SYSTEM PERFORMANCE COMPARATIVE ANALYSIS

To examine the performance of the constructed digital twin textile process system in key performance areas, this section introduces four representative systems serving as comparative baselines from two evaluation dimensions. COLMAP and OpenMVS are adopted as reconstruction and texture mapping algorithms, reflecting the accuracy dimension of geometric modeling and texture fidelity. Vicon and Unity-based simulation platforms represent the interaction dimension, focusing respectively on high-precision motion trajectory capture and process-level interactive visualization. All experiments were conducted under a unified environment comprising an Intel Core i9-13900K processor, 64 GB DDR5 memory, and an NVIDIA RTX 4090 GPU. The rendering and interaction environment was provided through Chrome with WebXR and WebGL 2.0 support, operating within a Gigabit LAN. Single-user interaction was extended to a thirty-client concurrency simulation through load balancing to ensure consistency in comparative conditions. On this basis, the evaluation covered geometric error, response latency, and platform stability, with the results presented in Figure 7.

Experimental results showed that the proposed system achieved a point cloud overlap rate of 94.2%, exceeding COLMAP's 88.5% and OpenMVS's 86.7%, and significantly outperforming Vicon's 80.3% and Unity's 78.9%,

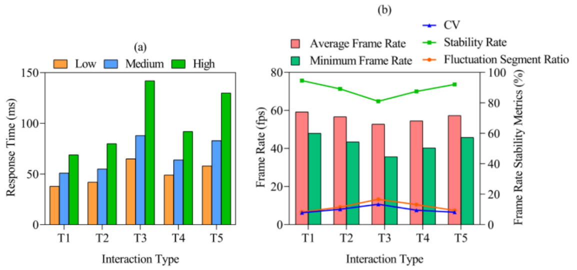

FIGURE 5. User interaction performance test results comparison. (a) Typical interactive operation response delay comparison, (b) Interactive task frame rate stability analysis, (c) Resource loading subprocess time-consuming structure diagram

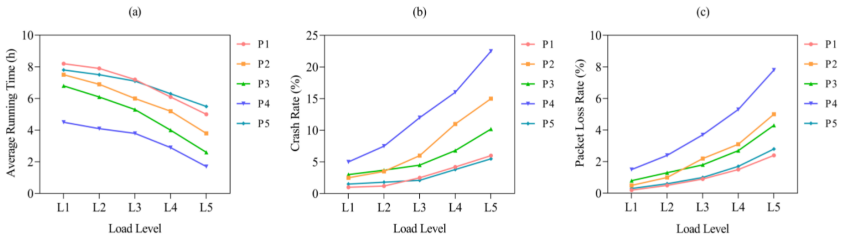

FIGURE 6. Comparison of system operation stability under platform and load conditions. (a) Comparison of average operation time, (b) Comparison of system crash rate, (c) Comparison of data packet loss rate

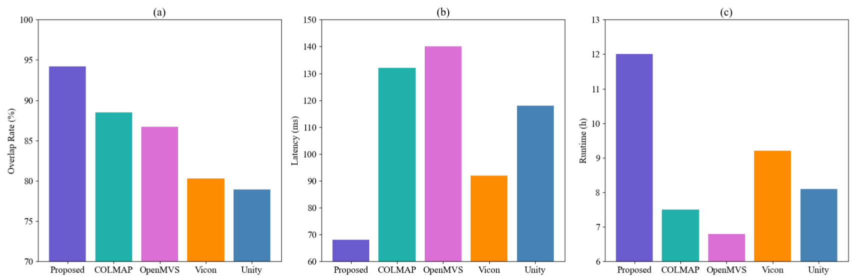

FIGURE 7. System performance comparison analysis results, (a) comparison of point cloud overlap rates of each system, (b) comparison of interaction delays of each system, (c) comparison of total operating time of each system

respectively. This improvement is attributed to the integration of laser scanning and multi-view data in the modeling phase, enabling more complete geometric reconstruction. Regarding interactive performance, the proposed system's latency was 68 milliseconds, lower than Vicon's 92 milliseconds and Unity's 118 milliseconds, while COLMAP and OpenMVS both exceed 130 milliseconds. This reflects the effectiveness of its data flow optimization and WebXR rendering synchronization strategy. In terms of operational stability, the proposed system supported 12 hours of continuous operation, exceeding Vicon's 9.2 hours and Unity's 8.1 hours, and surpassing those of COLMAP and OpenMVS (both < 8 h). This advantage is attributed to improvements in backend database management and resource scheduling mechanisms. A comprehensive comparison shows that the proposed system excels in accuracy, responsiveness, and stability.

ANALYSIS OF COMMUNICATION EFFECTIVENESS EVALUATION INDICATORS

After the digital twin system was constructed, a series of comparative end-user experience experiments were designed to further explore its performance in user cognitive guidance and interactive communication. Data were collected and analyzed based on five indicators: craft understanding accuracy, cultural perception score, average interaction time, social sharing rate, and repeat visit rate. These indicators reflect the system's comprehensive impact on user acquisition of intangible cultural heritage knowledge, cultural semantic acceptance, platform stickiness, and content diffusion potential. Craft understanding accuracy quantifies the user's mastery of key knowledge points such as process nodes and tool functions; cultural perception score reflects the user's subjective understanding of the cultural background and context of the craft from a cognitive psychological perspective; average interaction time reflects the user's willingness to engage with content on the platform; and social sharing rate and repeat visit rate are key metrics for measuring the system's activeness and user return across multiple rounds of communication. The data were collected from 50 participants who took part in the user experience experiment. Each participant completed pre- and postexperiment surveys and system-based interactions, with logs automatically recorded to capture behavioral indicators. The dataset consisted solely of anonymized interaction records and structured questionnaire responses, ensuring that the evaluation focused on usage performance and cultural cognition outcomes. The results are summarized in Table 3.

TABLE 3. Comparative experimental results of user cognition and dissemination behavior

Indicator Name	Pre-Experience Value	Post-Experience Value	Increase/Change
Craft Understanding Accuracy	68.5%	91.2%	↑22.7%
Cultural Perception Score	3.2/5	4.4/5	↑1.2
Average Interaction Duration	3 min 26 s	6 min 21 s	↑85.0%
Social Sharing Rate	12.5%	27.6%	↑15.1%
Repeat Visit Rate	20.3%	35.1%	↑14.8%

Experimental results showed that after users completed the system experience, their accuracy in understanding craftsmanship improved to 91.2%. This performance is closely related to the craftsmanship logic chain constructed by 3D dynamic modeling and immersive interactive structures. Its multimodal expression pathway enables users to gradually construct an active understanding of craft nodes and instrument functions during operation. Cultural perception scores steadily improved, thanks to the platform's metadata linkage mechanism between semantic annotation and pattern structure, which effectively enhances users' perception of the cultural encodings behind craftsmanship. The significant increase in average interaction time indicates that the system has a high level of operational appeal in terms of action response latency, visual feedback continuity, and information density distribution, significantly enhancing user engagement. Increased social sharing and repeat visit rates indicate that the platform has a certain influence on user communication. This result is related to the system's low-threshold WebXR deployment strategy and the adaptive reconstruction of node-based knowledge structures, which enhance its fluidity and revisitability within non-rigid communication pathways. Comprehensive analysis confirms that the system demonstrates a synergistic and reinforcing communication effectiveness mechanism in activating user craftsmanship cognition, deepening cultural acceptance, and driving communication behavior.

VI. CONCLUSION AND DISCUSSION

LIMITATIONS AND CHALLENGES

Although the proposed system establishes an integrated framework and achieves favorable results, several limitations remain evident. The modeling and synchronization strategies developed in this study are primarily suited to crafts with structured motions and repeatable operational cycles. This restricts their generalization to practices characterized by irregular trajectories or non-standardized force patterns. Substantial variation in motion amplitude and unpredictable tool–fabric interactions increase instability in motion capture accuracy and reduce the reliability of predictive correction, thereby complicating the maintenance of synchronization fidelity. Divergences in execution style among artisans, manifested in differences in motion rhythm, gesture magnitude, and process segmentation, further compromise metadata consistency and semantic alignment, limiting system robustness outside controlled experimental settings. In addition, the scalability of the metadata framework is constrained, as its current implementation depends on expert validation for annotation and correction, hindering its extension to large-scale heterogeneous datasets. Future research should address these challenges through adaptive calibration mechanisms, context-aware motion generalization methods, and semi-automated semantic annotation processes, thereby enhancing the applicability of the system to a broader spectrum of crafts and improving resilience to inter-operator variability.

CONCLUSION

This paper addresses the bottleneck of digital communication in textile intangible cultural heritage by developing a digital twin system that integrates dynamic modeling, behavior capture, and immersive interaction. High-fidelity 3D models are reconstructed using laser scanning and multi-view photogrammetry; IMU arrays captured key action nodes for skeleton-driven mapping; and a WebXR-based terminal supported immersive interaction, forming a closed-loop from action semantics to visual feedback. Experimental results demonstrated strong performance: under high-density sampling, point cloud overlap reached 94.2%, and COLMAP reconstruction achieved a geometric error below 0.40 mm, indicating high structural fidelity. In dynamic simulation, brocade crafts show frame synchronization rates exceeding 90% at "acceleration," "turning," and "deceleration" nodes, validating the rhythm-matching mechanism. For interactive performance, model rotation under high load responded within 70 ms, with frame-rate variation was below 8%, ensuring real-time interaction. Overall, the method enables closed-loop mapping of "craft–action– semantics" and supports visualization, operational restructuring, and sustainable cross-platform communication of traditional knowledge. Nevertheless, the present system exhibits limitations in scaling to highly irregular crafts and in adapting to executional variations among different artisans. These constraints highlight the need for adaptive synchronization strategies and scalable semantic modeling in subsequent research, paving the way for broader applicability and higher resilience of digital heritage communication systems.

AUTHOR CONTRIBUTIONS

All work in this study was independently completed by Wei ZHAO.

CONFLICTS OF INTEREST

The author declares no conflict of interest.

FUNDING

This study was supported by the General Project of Humanities and Social Sciences Research in Henan Province Colleges and Universities, titled "Research on the Cultural Memory Activation Mechanism of Intangible Cultural Heritage Short Videos under Embodied Cognition "(2026-ZDJH-931)

ACKNOWLEDGEMENTS

Not applicable.

REFERENCES

[1] L. Yu, “Digital Sustainability of Intangible Cultural Heritage: The Example of the “Wu Leno” Weaving Technique in Suzhou, China,” Sustainability, vol. 15, no. 12, pp. 9803-9819, 2023.
[2] Y. Huang, J. Chang, and G. Li, “Framework for Digital Transformation of Intangible Cultural Heritage: Chinese Paper-Cutting Art,” Archives of Design Research, vol. 37, no. 1, pp. 43-58, 2024.
[3] X. Zabulis, C. Meghini, A. Dubois, P. Doulgeraki, N. Partarakis, I. Adami, et al., “Digitisation of traditional craft processes,” Journal on Computing and Cultural Heritage (JOCCH), vol. 15, no. 3, pp. 1-24, 2022.
[4] N. Partarakis, V. Doulgeraki, E. Karuzaki, G. Galanakis, X. Zabulis, C. Meghini, et al., “A web-based platform for traditional craft documentation,” Multimodal Technologies and Interaction, vol. 6, no. 5, pp. 37-69, 2022.
[5] B. Yu, L. Fang, L. Luo, X. Hu, and C. Shen, “A Study on Service-Oriented Digital Twin Modeling Methods for Weaving Workshops,” Machines, vol. 12, no. 8, pp. 542-565, 2024.
[6] L. Lu and M. Li, “Development of a virtual interactive system for Dahua Lou loom based on knowledge ontology-driven technology,” Heritage Science, vol. 11, no. 1, pp. 178-192, 2023, doi: 10.1186/s40494-023-01027-x.
[7] L. Zhang, Y. Wang, Z. Tang, X. Liu, and M. Zhang, “A virtual experience system of bamboo weaving for sustainable research on intangible cultural heritage based on VR technology,” Sustainability, vol. 15, no. 4, pp. 3134-3150, 2023.
[8] R. Yang, Y. Li, Y. Wang, Q. Zhu, N. Wang, Y. Song, et al., “Enhancing the Sustainability of Intangible Cultural Heritage Projects: Obtaining Efficient Digital Skills Preservation through Binocular Half Panoramic VR Maps,” Sustainability, vol. 16, no. 13, pp. 5281-5299, 2024.
[9] F. Niccolucci, A. Felicetti, and S. Hermon, “Populating the data space for cultural heritage with heritage digital twins,” Data, vol. 7, no. 8, pp. 105-133, 2022.
[10] A. Felicetti and F. Niccolucci, “Artificial Intelligence and Ontologies for the Management of Heritage Digital Twins Data,” Data, vol. 10, no. 1, pp. 1-25, 2024.
[11] M. T. Artese and I. Gagliardi, “Integrating, indexing and querying the tangible and intangible cultural heritage available online: the QueryLab portal,” Information, (2022), 13(5), 260-280.
[12] F. Niccolucci and A. Felicetti, “Digital Twin Sensors in Cultural Heritage Ontology Applications,” Sensors, vol. 24, no. 12, pp. 3978-3998, 2024.
[13] P. Hui Han, X. Rong Li, R. Liu, S. Zhang, and C. Yuan, “Prediction method of carding process production quality based on digital twin technology,” Textile Research Journal, vol. 94, no. 5-6, pp. 713-724, 2024.
[14] M. Li, S. Xu, J. Tang, and W. Chen, “Design and research of digital twin platform for handicraft intangible cultural heritage-Yangxin Cloth Paste,” Heritage Science, vol. 12, no. 1, pp. 43-65, 2024, doi: 10.1186/s40494-024-01161-0.
[15] S. Wang, X. Deng, and M. Zhang, “Digital Reconstruction and Display of Intangible Cultural Heritage based on CAD Modeling and Reinforcement Learning,” Comput. Aided Des. Appl, vol. 21, no. 1, pp. 117-133, 2024.
[16] Y. Liu, “Application of digital technology in intangible cultural heritage protection,” Mobile Information Systems, vol. 2022, no. 1, pp. 7471121-7471129, 2022.
[17] K. Ban, Y. Huai, X. Nie, Q. Meng, and H. Xu, “SAGS-GNN: Graph Neural Network for self-collision and anisotropy in dynamic garment simulation,” Computers & Graphics, vol. 128, no. 1, pp. 104216-104232, 2025.
[18] X. Jing, F. Tan, and M. Zhang, “Digital application of intangible cultural heritage from the perspective of cultural ecology,” Journal of Smart Tourism, vol. 1, no. 1, pp. 41-52, 2021.
[19] M. A. R. HassanArchitecture, A. M. al-Moqaram, and B. S. Ali, “The Role of Digital Craftsmanship by “Hybrid Re-Assemblage” Technique in The Restoration of Historical Buildings,” Ilkogretim Online, vol. 21, no. 3, pp. 79-97, 2022.
[20] M. Chiachío, M. Megía, J. Chiachío, J. Fernandez, and M. L. Jalón, “Structural digital twin framework: Formulation and technology integration,” Automation in Construction, vol. 140, pp. 104333-104345, 2022.
[21] W. Luther, N. Baloian, D. Biella, and D. Sacher, “Digital twins and enabling technologies in museums and cultural heritage: An overview,” Sensors, vol. 23, no. 3, pp. 1583-1611, 2023.
[22] A. Amelio and G. P. Zarri, “Cultural heritage digital twin: Modeling and representing the visual narrative in Leonardo da Vinci’s Mona Lisa,” Neural Computing and Applications, vol. 36, no. 20, pp. 11859-11876, 2024.
[23] A. Shabani, M. Skamantzari, S. Tapinaki, A. Georgopoulos, V. Plevris, and M. Kioumarsi, “3D simulation models for developing digital twins of heritage structures: Challenges and strategies,” Procedia Structural Integrity, vol. 37, no. 1, pp. 314-320, 2022.
[24] W. Ning, “Innovative frameworks for protecting intangible cultural heritage using advanced multimedia technology drawing on digital twins and 3D modeling,” Intelligent Decision Technologies, vol. 19, no. 2, pp. 1023-1039, 2025.